

Effects of aluminum distearate addition on UO_2 sintering and microstructure

Artur Cesar de Freitas^a, Diogo Ribeiro Costa^{b,1}, Paula Mendes Jardim^b,
Ricardo Mendes Leal Neto^a, Elita Fontenele Urano de Carvalho^a, Michelangelo Durazzo^{a,*}

^a Nuclear and Energy Research Institute – IPEN/CNEN-SP, São Paulo, Brazil

^b Department of Metallurgical and Materials Engineering, - UFRJ/COPPE, Rio de Janeiro, Brazil

ARTICLE INFO

Keywords:

UO_2 fuel
Aluminum distearate
Sintering behavior
Grain growth

ABSTRACT

Uranium dioxide (UO_2) is widely used as a fuel in commercial nuclear light-water reactors (LWRs). Rigorous control of density, pore, and grain size of UO_2 pellets are important prerequisites for fuel performance. Solid lubricants, frequently used in pellets manufacturing, minimize structural defects on compaction such as cracks and end-capping, promoting grain growth during sintering. This work presents and discusses the effects of the aluminum distearate (ADS) addition on the sintering behavior and microstructure of UO_2 fuel pellets. UO_2 and UO_2 -0.2wt% ADS pellets were sintered at 1760 °C for 5.7 h for comparison purposes. The results show that the densification rate increases using the solid lubricant, but the shrinkage is lowered by 0.7% due to low homogenization. The average grain size was increased by about 35% during sintering. Based on our results and a literature review, a mechanism for grain growth by aluminum addition is proposed.

1. Introduction

Uranium dioxide (UO_2) nuclear fuel has been widely used in commercial light water reactors (LWRs), such as boiling (BWR) and pressurized (PWR) water reactors (Olander, 2009; IAEA – International Atomic Energy Agency, 2012). UO_2 combines its high melting point with low swelling under irradiation, good water-resistance corrosion, and economical production from enriched uranium hexafluoride (OECD Nuclear Energy Agency, 2014; Lyons et al., 1972). In Brazil, UF_6 enrichment is done by ultracentrifugation at the Nuclear Industries of Brazil (INB, Indústrias Nucleares do Brasil S.A.). UO_2 powder is produced via the ammonium uranyl carbonate (AUC) wet route (Costa and Freitas, 2017). The AUC powder is produced from the UF_6 hydrolysis and then reduced to UO_2 under a hydrogen and superheated steam atmosphere. The advantage of this route is the production of free-flowing and sinterable (high specific surface area) UO_2 powder, suitable to be pressed and sintered, requiring no intermediate steps such as milling, prepressing, or sieving before sintering (Santos et al., 2017).

Regarding the requirements for long fuel performance, fission products can affect dimensional stability, mechanical properties,

thermal conductivity, melting point, and chemical reactivity (Belle, 1961; Olander, 1976). The fuel's ability to retain fission products is then of paramount importance. Among them, gaseous and volatile products constitute a significant concern since they are able to spread through pellets, which are the first barrier to their release. This is particularly the case of xenon and krypton, which are poorly dissolved in the UO_2 matrix and thus are hardly retained inside the pellets. Besides this safety issue, released gaseous fission products to the plenum are detrimental to the thermal conductivity of the fuel-cladding gap, impairing the thermal behavior of the fuel rods, especially on an extended burn-up range (Rest et al., 2019).

Due to its relevance for fuel performance, fission gas release (FGR) mechanisms have been studied for a long. Generally, FGR can be summarized through three stages (Tonks et al., 2018). First, gas atoms are produced and transported through the bulk of the grain; second, bubbles nucleate at the grain faces, grow by the migration of other gas atoms to existing bubbles, and coalesce with each other until they reach grain edges; third, gas is released to free surfaces by the transport through interconnected grain edges channels. Despite remaining open questions about these stages, it is clear that grain size control is critical for FGR

* Corresponding author. 2242, Cidade Universitária, CEP, 05508, São Paulo, SP, Brazil.

E-mail addresses: artur.freitas@ipen.br (A. Cesar de Freitas), diogorc@kth.se (D.R. Costa), pjardim@metalmat.ufrj.br (P.M. Jardim), lealneto@ipen.br (R.M. Leal Neto), elitaucf@ipen.br (E.F. Urano de Carvalho), mdurazzo@ipen.br (M. Durazzo).

¹ Currently at KTH Royal Institute of Technology, Division of Nuclear Engineering, Stockholm, Sweden.

reduction (Radford and Pope, 1983; Olander, 2009). Larger grains are preferred since the path for the fission gas atoms to migrate to grain faces and nucleate bubbles is increased.

Conversely, a microstructure with small grains facilitates the release of gases from the pellet. The smaller the grain size, the greater the grain boundary area and the shorter the diffusional path for the fission products to escape via grain boundary diffusion (Turnbull, 1974). Pellets with large grain sizes are softer, which is good for lowering the intensity of the pellet-cladding mechanical interaction (PCMI), decreasing the risk of cladding failure (Leckie and Luther, 2013; Massih, 2014).

UO₂ pellet grain size can be enlarged by increasing sintering temperature and time, but this procedure would raise industrial costs. So, one alternative that has been used for a long to increase the grain size, besides promoting higher sintered densities and enhanced plasticity, is doping the fuel with sintering additives, e.g., Al₂O₃, MgO, Cr₂O₃, Nb₂O₅. These additives (or dopants) act by forming solid solutions with UO₂ that change point defects concentration and affect the diffusion (thermophysical) properties of the fuel (Kashibe and Une, 1998; Leckie and Luther, 2013; Massih, 2014; Massih and Jernkvist, 2021).

The doping technology has been applied by some industries worldwide. Nevertheless, introducing chemical additives in UO₂ fuel could change the in-reactor pellet performance, which requires long-term verifications of the fuel pellet performance. Westinghouse's researchers have developed the ADOPT (Advanced Doped Pellet Technology) fuel (Arborelius et al., 2006). In this fuel concept, the UO₂ is doped with Cr₂O₃ and Al₂O₃ (the concentration is limited to 1,000 ppm) to enhance pellet densification during sintering, increasing grain size and reducing costs. According to the authors, aluminum oxide has little influence on the densification. It is, to some extent, used as a substitute for chromium oxide to reduce the parasitic neutron absorption induced, especially by chromium. Areva NP developed a UO₂ fuel doped with 0.16% of Cr₂O₃ (Delafoy and Dewes, 2006). High densities (96–97 %TD) and large grain sizes (50–60 μm) were achieved in this fuel. In the development carried out by KEPCO Nuclear Fuel (KNF) and Korea Atomic Energy Research Institute (KAERI) (Lee et al., 2011), 30 ppm of Al₂O₃ was added to the UO₂ fuel, mixed with low-temperature-oxidized U₃O₈ (350 °C), increasing the average grain sizes from 7 to 8 μm, with high-temperature oxidized U₃O₈ (450 °C) and no Al₂O₃, to 15–18 μm. When Al₂O₃ was added to UO₂ with high-temperature-oxidized U₃O₈, the measured grain size was 11.2 μm (Yang et al., 2010).

Besides changing the thermophysical properties, such as enthalpy, thermal capacity, thermal expansion, and thermal conductivity, the use of sintering additives may damage the neutronic performance of the fuel, so long-term verifications of the fuel pellet performance are required. For this reason, dopant content was generally restricted to no more than 0.5 wt% (Massih, 2014).

As an example, INB has restricted specification limits for some chemical elements' maximum impurity (Durazzo et al., 2018), as reported in Table 1.

Among the various sintering additives used, aluminum is particularly interesting in this work. Different materials have been chosen as sources of aluminum, as shown in Table 2.

Aluminum oxide, or alumina (Al₂O₃) (Flipot et al., 1973; Kashibe and Une, 1998; Hua et al., 2004; Yang et al., 2010; Lee et al., 2011; Zhong et al., 2021), and aluminum hydroxide, Al(OH)₃ (Schafer et al., 1984; Assmann et al., 1988; Santos et al., 2017) have been used more extensively. It is not uncommon to have an aluminum source used with another additive (co-dopant), such as Cr₂O₃ (Kashibe and Une, 1998; Arborelius et al., 2006), SiO₂ (Matsuda et al., 1998; Hua et al., 2004), or

even MnO (Kang et al., 2010). As shown in Table 2, aluminum addition promotes a slight variation in UO₂ pellet density. The grain size, on the other hand, increases about two times. No increase was reported by Zhong et al. (2021). However, in that case, pure UO₂ powder was ball milled before sintering (as UO₂ plus the additive), which certainly promoted intense mechanical activation, concealing the effect of aluminum doping. Higher grain size growth is observed when a co-dopant is used, as with Cr₂O₃ (Arborelius et al., 2006), SiO₂ (Matsuda et al., 1998; Hua et al., 2004), or silicate (Yuda et al., 1997; Une et al., 2000). In some cases, intergranular eutectic phases were reported to become liquid at the sintering temperature, promoting high diffusion rates at the grain boundaries (Matsuda et al., 1998; Yuda et al., 1997; Kang et al., 2010), increasing grain size by around five times. Flipot et al. (1973) reported a eutectic liquid phase in Al₂O₃ doped UO₂ with Dy₂O₃, but in that case, sintering was carried out at an extremely high temperature (1915 °C), providing UO₂-Al₂O₃ eutectic liquid.

In Table 2, special attention must be devoted to the aluminum hydroxide distearate (AlOH(C₁₈H₃₅O₂)₂) (Jentzen and Didway, 1990), or simply aluminum distearate (C₃₆H₇₁AlO₅) (Yaws, 2015), whose acronym is ADS. Besides being an aluminum precursor, this material is rather known for its lubricant properties. Solid lubricants such as stearic acid, uranyl stearate, and zinc stearate are commonly used to improve powder compaction, particularly brittle ceramics such as UO₂ powder. These carbon-based compounds decrease the friction between particle-particle and particle-die walls and diminish the springback behavior when the pellet is removed from the die (Jentzen and Didway, 1990; Klemm and Sobek, 1989). Therefore, cracks and end-capping defects in the green pellet may be minimized or even eliminated using a solid lubricant (Balakrishna et al., 1999). Comparing ADS with zinc stearate, the ADS has shown to be more effective in improving green pellet strength, besides acting as a grain size enhancer (Jentzen and Didway, 1990). Jentzen and Didway (1990) reported that mixtures of 0.1–0.4 wt% ADS in UO₂ were homogenized in a Turbula mixer for 5–15 min and subsequently sintered in a temperature range between 1700 °C and 1780 °C in H₂/H₂O atmosphere (dew point between 21 and 35 °C) for 2–3 h. By doing so, the authors claimed that the distearate radical is removed as a fugitive during sintering. The aluminum metal remains as an hydroxide component, which is converted to aluminum oxide. However, neither grain size nor density variation measurements were presented. ADS was also utilized later as an aluminum precursor since, upon sintering, it was expected to convert to its oxide form (Leckie and Luther, 2012, 2013). Near the solubility limit of 100 ppm Al₂O₃, the grain size increase about two times while a little increase is seen on sintered density. Costa et al. (2013) added Al₂O₃ to UO₂+ADS samples. It was seen that the density of the sintered pellets decreased almost linearly with the Al₂O₃ addition, which is compatible with the lower density of alumina itself. There was reported just a marginal increase in grain size up to 0.3 wt% Al₂O₃ since the reference material already had 0.2 wt% ADS. Actually, the average grain size fluctuates with alumina addition, which is consistent with the error range of the measurements.

It is clear that besides being a solid lubricant, ADS is also a source of aluminum ions that will be solved in UO₂, enhancing sintering and promoting grain growth. To better understand this behavior, detailed investigations of the impact of ADS addition on the sintering, microstructure, and thermal stability of UO₂ fuel during resintering are presented in the present study. Mixtures of 0.2 wt% ADS and UO₂ powder were sintered at 1760 °C for 5.7 h and compared with pure UO₂ fuel. The resintering test was chosen here because it correlated with the stability of the UO₂ pellets during thermal heating in operation, which is

Table 1

INB specification for the maximum impurities in the UO₂ powder.

Impurity (μg/gU)	F	Al	Ca	B	Fe	Ni	Si	Gd
Specification limits	≤100	≤250	≤25	≤0.5	≤100	≤50	≤100	≤1

Table 2

Density and grain size values from various UO₂-base nuclear fuels compared with those attained by adding different aluminum precursors as a sintering aid. Density and grain size values correspond to the maximum attained in each case. In base material and base material + additive columns. U₃O₈ is from high and low-temperature oxidation, respectively (n.r. = not reported; T.D. = theoretical density; ADS = aluminum hydroxide distearate).

ALUMINUM SOURCE (amount)	Base Material	DENSITY (g/cm ³ or %T.D.)		GRAIN SIZE (μm)		Reference
		Base Material	Base Material + additive	Base Material	Base Material + additive	
Al ₂ O ₃ (120 ppm Al-coprecipitated UO ₂)	UO ₂ + Dy ₂ O ₃	n.r.	n.r.	n.r.	n.r.	Flipot et al. (1973)
Al(OH) ₃ (80 ppm by weight)	UO ₂ + PuO ₂ + Gd ₂ O ₃	93.4 %T.D.	95.7 %T.D.	n.r.	n.r.	Schafer et al. (1984)
Al(OH) ₃	UO ₂ + Gd ₂ O ₃	9.93	10.17	n.r.	n.r.	Assmann et al. (1988)
ADS	UO ₂ + U ₃ O ₈	n.r.	(increase) n.r.	n.r.	(increase) n.r.	Jentzen and Didway (1990)
Al ₂ O ₃ + SiO ₂ (0.04wt%)	UO ₂	10.55	10.55	9	28	Matsuda et al. (1998)
Alumino-Silicate (0.25wt%)	UO ₂	97.17 %T.D.	97.79 %T.D.	9	46	(Yuda et al., 1997; Une et al., 2000)
Al ₂ O ₃	UO ₂	10.71	10.70	15	30	Kashibe and Une (1998)
Al ₂ O ₃ (100 ppm)	UO ₂	10.387	10.483	8.0	21.6	Hua et al. (2004)
Al ₂ O ₃ + SiO ₂ (200 ppm)	UO ₂	10.387	10.483	8.0	26.2	Hua et al. (2004)
Al ₂ O ₃ + Cr ₂ O ₃	UO ₂	10.60 (96.7 %T.D.)	10.67 (97.3 %T.D.)	10–12	40–55	Arborelius et al. (2006)
Al(NO ₃) ₃ .9H ₂ O (~42 ppm Al)	UO ₂	n.r.	n.r.	7.7	12	Kim (2007)
Al ₂ O ₃ (40 ppm at wt. ratio of Al/U)	UO ₂ + U ₃ O ₈ + Al ₂ O ₃	10.79	10.77	11.2	16.6	Yang et al. (2010)
95MnO-5Al ₂ O ₃ (mol%) (1000 ppm)	UO ₂	n.r.	n.r.	8	51	Kang et al. (2010)
Al ₂ O ₃ (30 ppm)	UO ₂ + 8 wt% U ₃ O ₈	95.8%T.D.	95.7%T.D.	7–8	15–18	Lee et al. (2011)
ADS (100 ppm Al ₂ O ₃)	UO ₂	93.9 %T.D.	94.5 %T.D.	5.75	10.1	Leckie and Luther (2012)
Al ₂ O ₃ (0.3 g Al/g U)	UO ₂ + ADS	10.58	10.47	12.5	14.5	Leckie and Luther (2013)
Al(OH) ₃ (0.2wt%)	UO ₂ + Gd ₂ O ₃	9.81	10.18	4.4	10.4	Costa et al. (2013)
Al ₂ O ₃ nano (100 ppm)	UO ₂	n.r.	n.r.	16	16	Santos et al. (2017)
						Zhong et al. (2021)

fundamental for predicting dimensional behavior during irradiation of UO₂ fuel pellets (Costa and Freitas, 2017; Maier et al., 1988).

2. Materials and methods

2.1. Raw materials

INB supplied the UO₂ powder used in this study. Table 3 shows the physicochemical data of the UO₂ powder.

Morphological characteristics of UO₂ powder were observed on a Thermo Fisher Prisma E Scanning Electron Microscope (SEM) with secondary electrons (SE) detector. The particle size distributions were assessed by laser diffraction method using CILAS laser equipment

Table 3
Physicochemical data of the UO₂ powder.

Characteristics	Results	Specification
O/U	2.08	2.08–2.30
U _{total} (%)	87.6	≥86.8
Enrichment U-235 (%)	4.14	4.10–4.15
Moisture (wt%)	0.2	≤0.4
Surface area (m ² /g)	5.0	2.5–6.0
Bulk density (g/cm ³)	2.2	2.0–2.6
Flowability (s/50 g) ^a	4.6	≤10
Mean particle size (μm)	30	<200
Impurities (μg/gU)		
F	5.3	≤100
Al	1.8	≤250
Ca	4.2	≤25
B	<0.2	≤0.5
Fe	15.2	≤100
Ni	0.4	≤50
Si	6.9	≤100
Gd	0.2	≤1

^a 50 g of material must flow through a standard glass funnel at an angle of 10° in less than 10s.

(model 1064), with water as the liquid medium and tetrasodium pyrophosphate as a dispersant agent. The UO₂ powder morphology is characteristic of the industrial AUC wet route (Durazzo et al., 2018), with different particle sizes (~2–100 μm). Fig. 1 presents a typical SEM image of the UO₂ powder.

The UO₂ powder has a monomodal distribution, with D50 equal to 30.0 μm. Fig. 2 shows the particle size distributions of the UO₂ powder.

The ADS powder was supplied by Sigma-Aldrich (4.5–6 wt% Al basis, product number 26402). Thermogravimetric analysis (TG) of the ADS powder was first carried out in the air for residue on ignition (ashes) determination, as shown in the decomposition curve of Fig. 3A. After heating up to 1000 °C, the residue on ignition was 10.34 wt%, which is within the manufacturer specification range (10–12 wt%). We also ran a thermal analysis under an H₂ atmosphere with a similar heating program to that used in the sintering of the pellets (6 °C/min up to 1500 °C). The result is presented in Fig. 3B. Weight loss started at about 180 °C and stabilized around 650 °C, corresponding to an 87.81 wt% variation. At 1500 °C, the residue was 12.19 wt%, indicating that the reaction under hydrogen differs from the air. Thermal decomposition of ADS proved to be quite complex, both under air and H₂ atmospheres. The decomposition under H₂ showed at least three main events involving mass change, as shown by the first derivative curves. Decomposition under air proved even more complicated, with probably more than four events. As far as we know, only one reference deals with the thermal decomposition of aluminum stearate, which is dated to the sixties (Shiba, 1961). In that article, only differential thermal analysis results were presented and limited to 250 °C. A detailed study on this topic will be the subject of future work.

The ADS powder was also characterized by scanning electron microscopy (SEM). ADS particles (Fig. 4) have an irregular shape and are very fine, which favors the formation of large agglomerates (~40 μm). It was challenging to assure complete dispersion of ADS particles, so the particle size distribution in Fig. 5 should be rather regarded as an agglomerate size distribution. A multimodal distribution ranged from

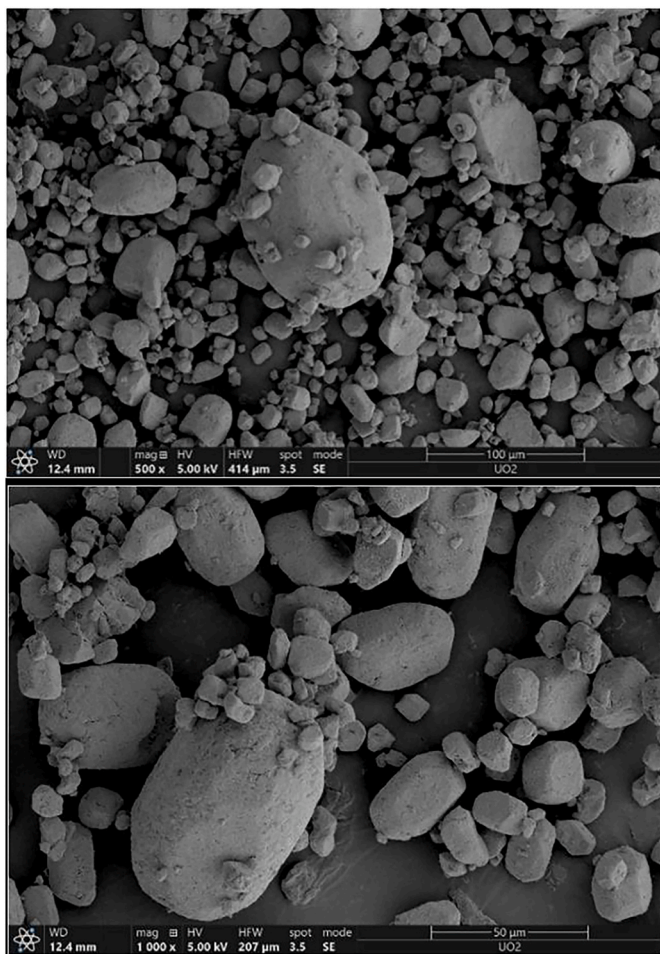


Fig. 1. SEM-SE images showing the morphology of UO_2 particles.

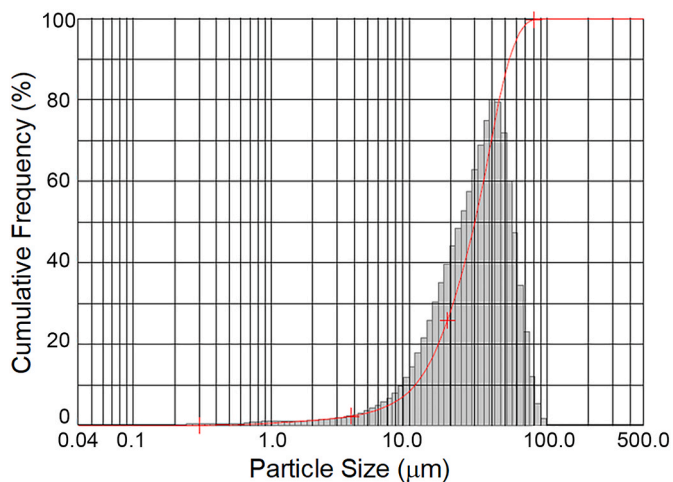


Fig. 2. Particle size distribution of UO_2 powder.

0.1 to 70 μm , with D50 equal to 12.6 μm .

2.2. Sample preparation and characterization

Mixtures of 0.2 wt% ADS and UO_2 powders were homogenized in a roller mixer for 30 min at 200 rpm. Afterward, pure UO_2 powder and the mixtures were compacted at 400 MPa with a uniaxial hydraulic press using a cylindrical die (11.20 mm internal diameter). The die walls were

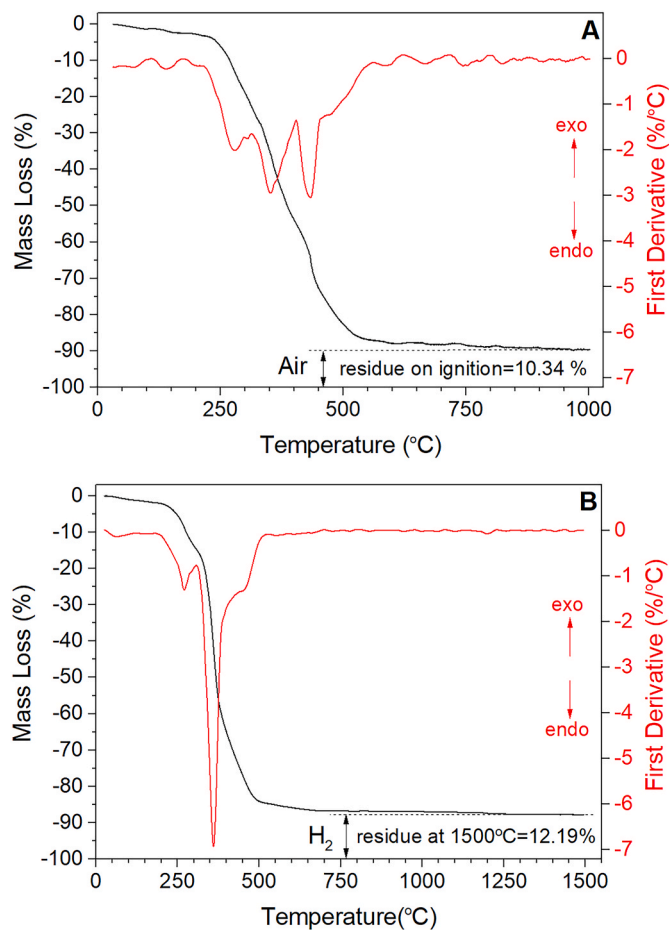


Fig. 3. Thermal decomposition curves of ADS powder used as raw material (Sigma-Aldrich) under air (A) and hydrogen (B).

lubricated with an oil film.

Green densities were measured by the geometric method, i.e., green pellets were individually weighed in a semi-analytical balance (0.0001 g), and their volume was determined assuming a cylindrical shape. The height and diameter of the pellets were measured with a 0.01 mm precision caliper. The theoretical density (TD) of the UO_2 -0.2 wt% ADS mixture was calculated based on the UO_2 and ADS individual TD values: 10.96 g/cm^3 (Turnbull, 1974; Delafoy and Dewes, 2006) and 1.01 g/cm^3 (Delafoy and Dewes, 2006; Balakrishna et al., 1999), respectively.

A total of ten UO_2 -ADS green pellets and ten pure UO_2 green pellets were simultaneously sintered using the INB industrial furnace (GWSmo 16/14/210) at 1760 $^\circ\text{C}$ for 5.7 h in humidified H_2 atmosphere, with a dew point of -30 $^\circ\text{C}$ ($\text{H}_2\text{O}/\text{H}_2 = 5.10^{-4}$, or $\text{H}_2 + 0.05\text{v}\text{H}_2\text{O}$). The sintering furnace has electrical resistances for heating, refractory insulators of ultra-purity alumina, and five different temperature zones: 500 $^\circ\text{C}$, 650 $^\circ\text{C}$, and three sintering zones at 1760 $^\circ\text{C}$. The movement of the samples throughout the 27 positions inside the furnace directly determined the heating rate and the sintering time at 1760 $^\circ\text{C}$. So, the resulting heating profiles were: 2.5 $^\circ\text{C}/\text{min}$ up to 650 $^\circ\text{C}$ and 6 $^\circ\text{C}/\text{min}$ until 1760 $^\circ\text{C}$, followed by 5.7 h at this plateau, and then cooling to room temperature at 6.5 $^\circ\text{C}/\text{min}$.

Sintered densities were measured by Archimedes' principle with water as the immersion medium in semi-analytical balance (0.0001 g) (ASTM, 2008). The densification behavior as a function of temperature, i.e., shrinkage curves, was assessed using a dilatometer SETARAM (Setsys 1700) in an H_2 atmosphere. The pellets were heated at 6 $^\circ\text{C}/\text{min}$ up to 1700 $^\circ\text{C}$, held at this temperature for 180 min, and then cooled at 20 $^\circ\text{C}/\text{min}$.

One sintered sample of each test was prepared for pore and grain

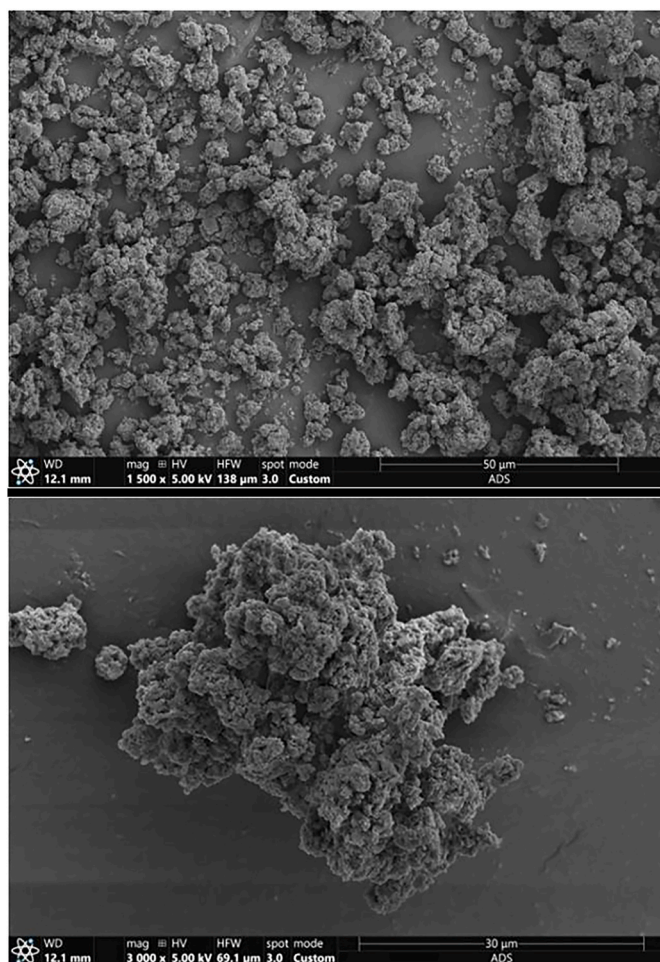


Fig. 4. SEM–SE images showing the morphology of ADS powder.

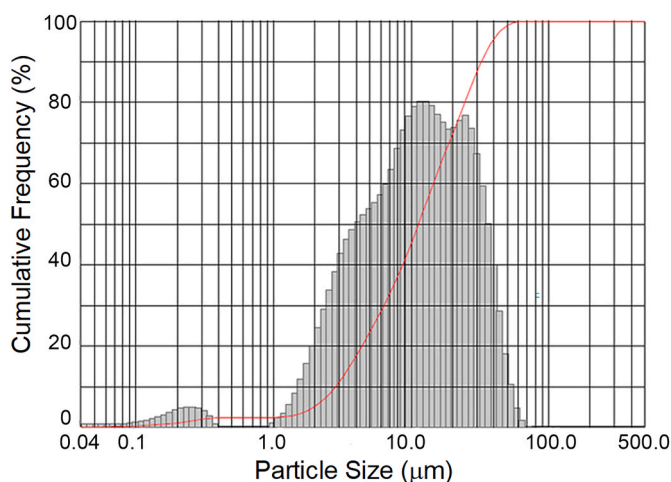


Fig. 5. Particle size distribution of ADS powder.

morphology investigations. The metallographic preparation included grinding with SiC paper (grid 400 and 1200) and polishing with diamond paste (3 μm and 1 μm). The average pore sizes of the polished samples were obtained using an optical microscope Olympus BX51M, with a magnification of 100X. In each sample, 10 images were used to calculate the average values (55,000 pores were measured). A thermal etching (1400 $^{\circ}\text{C}$, CO_2 , 1 h) of a polished surface was performed to

reveal the grain boundaries. The average grain sizes were obtained from 30 images per sample (5,000 grains were measured). The average length of pores and grains was calculated from different lengths in the same object (pore or grain) in intervals of 2° and passing through the centroid of each object. Ninety radial segments coming from the centroid were measured. The size of a particular grain is the average size of these radial segments. The value measured can be approximated to the diameter of a circle of the equivalent area of the grain section.

The thermal stability experiments, commonly named resintering test, were carried out at 1708 $^{\circ}\text{C}$ in a hydrogen atmosphere for 24 h. The industrial specification reports that the sample is classified as approved if the densification is higher than 0.2%TD and lower than 1.3%TD (Costa and Freitas, 2017). The “densification” is defined as the resintered density minus the sintered density. So, the density variation (%TD) was the ratio between the densification and the theoretical density of UO_2 .

3. Results

3.1. Effect of ADS addition on the green and sintered pellets

The use of lubricant is vital to avoid defects in the pellets. Fig. 6 shows a comparison between UO_2 pellets compacted without (Fig. 6A) and with 0.2 wt% of ADS (Fig. 6B). There are transversal cracks (lamination) and end-capping defects in the pellet without ADS, corroborating the lubricant’s importance in the specific manufacturing process used at INB.

The green and sintered densities and the theoretical densities of pure UO_2 and UO_2 -0.2 wt% ADS are presented in Table 4. Ten pellets of each sample were fabricated, aiming at $52 \pm 0.09\%$ TD (Costa and Freitas, 2017). Lubricant addition decreased the pore volume of the green samples compared to pure UO_2 samples (both compacted with the same pressure) since the relative densities (%TD) were higher. However, ADS sintered pellets presented lower densities.

One UO_2 -ADS sintered pellet was characterized for impurities determination. The results are presented in Table 5. Fig. 7 shows the XRD pattern for a UO_2 -ADS sintered pellet. It can be seen that the carbon content is very low. Aluminum content also is well below the specification limit. No uranium carbide was detected on the XRD pattern. No differences were observed in XRD patterns for pure UO_2 and UO_2 -0.2% wtADS.

3.2. Impact of ADS on the sintering behavior

The sintering behavior of UO_2 and UO_2 -0.2 wt% ADS is illustrated in Fig. 8. Fig. 8A shows that the addition of ADS decreased the total shrinkage from 19.9% (pure UO_2) to 19.4%. This reduction corroborates the reduction in sintered density reported in Table 4. Despite that, the lubricant caused an increase in the slope of the sintering curve, indicating that the shrinkage was accelerated by its addition.

Fig. 8B reports that the sample with ADS had a higher shrinkage rate and lower temperature at the maximum rate, shifting the temperature for the maximum shrinkage peak from approximately 1300 $^{\circ}\text{C}$ to 1270 $^{\circ}\text{C}$. The observed increase in the shrinkage rate may result from the Al^{3+} ions presented in the precursor. This observation will be commented on in the discussion section.

3.3. Influence of ADS addition on the microstructure of UO_2 fuel

3.3.1. Porosity analyses

Light optical microscopy images of UO_2 and UO_2 -0.2 wt% ADS are presented in Fig. 9A and B, respectively. The computed average pore sizes of the UO_2 and UO_2 -0.2 wt% ADS pellets are 2.92 μm and 2.75 μm , respectively.

In both cases, a ring-like pore shape can be observed. These pores were reported before and named half-moon pores (Costa et al., 2013).

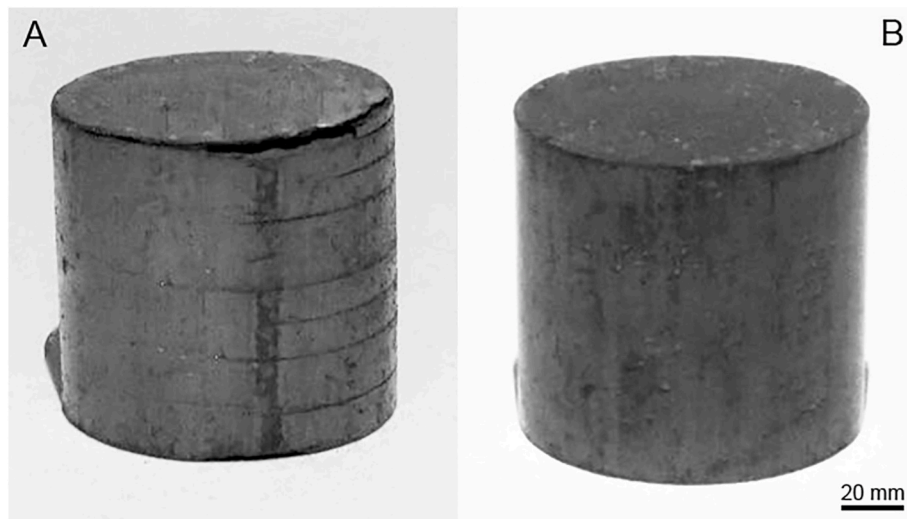


Fig. 6. Impact of ADS addition on the green pellet structure. The pellet compacted without ADS (A) showed cracks and end-capping defects. The addition of lubricant eliminated these defects (B).

Table 4
Green and sintered densities and the theoretical densities of pure UO_2 and UO_2 -0.2 wt% ADS.

Density	Pure UO_2	UO_2 -0.2wt% ADS
TD (g/cm^3)	10.96	10.75
Green density (g/cm^3)	5.70 ± 0.05	5.62 ± 0.05
%TD (green pellet)	52.01 ± 0.46	52.28 ± 0.47
Sintered density (g/cm^3)	10.61 ± 0.01	10.55 ± 0.01
%TD (sintered pellet)	96.81 ± 0.09	96.26 ± 0.09

Table 5
Impurity analysis results (ppm) for UO_2 -ADS sintered pellet.

Impurity	INB Specification	Results
Al	250	131
Ni	100	6.6
Ca	100	11
Fe	250	28
Si	100	26
Gd	3	0.2
C	100	30

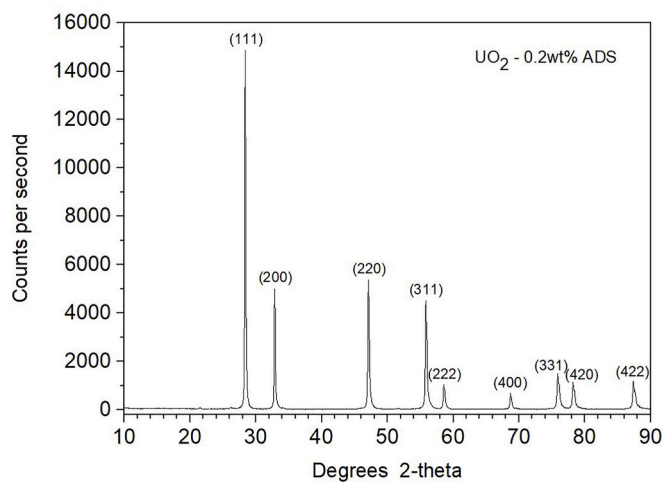


Fig. 7. X-ray diffraction pattern for sintered UO_2 -0.2wt% ADS pellet.

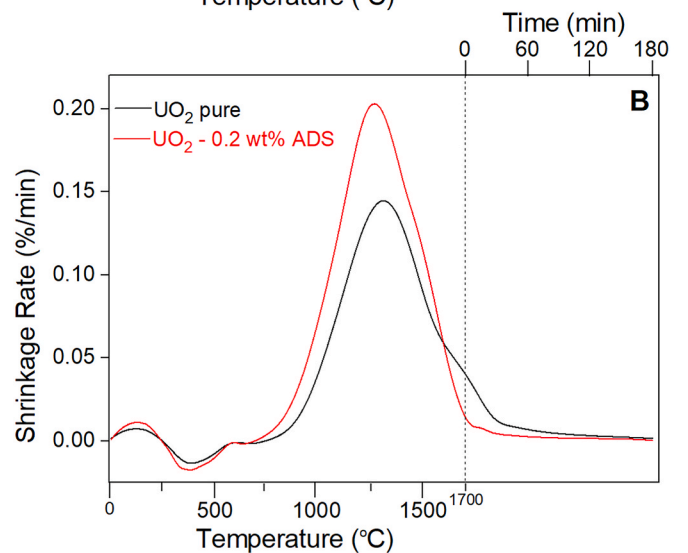
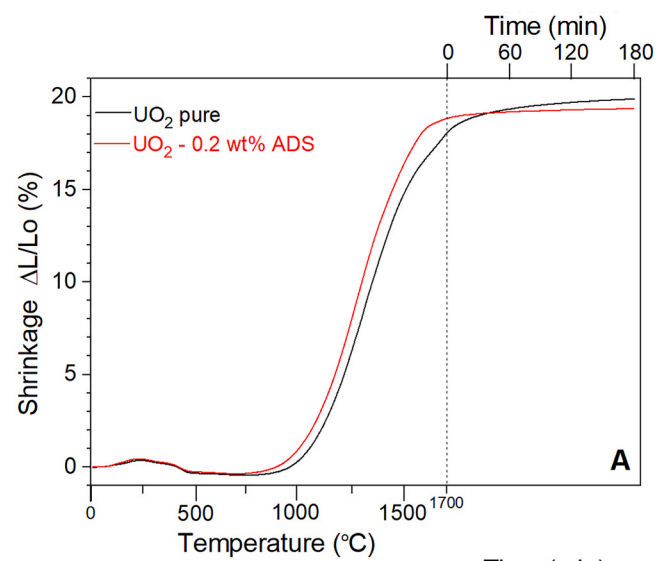


Fig. 8. Impact of ADS on the (A) sintering behaviors (shrinkage) and (B) shrinkage rates of pure UO_2 and UO_2 -0.2wtADS. The lubricant increased the maximum shrinkage rate and decreased the temperature at the maximum rate.

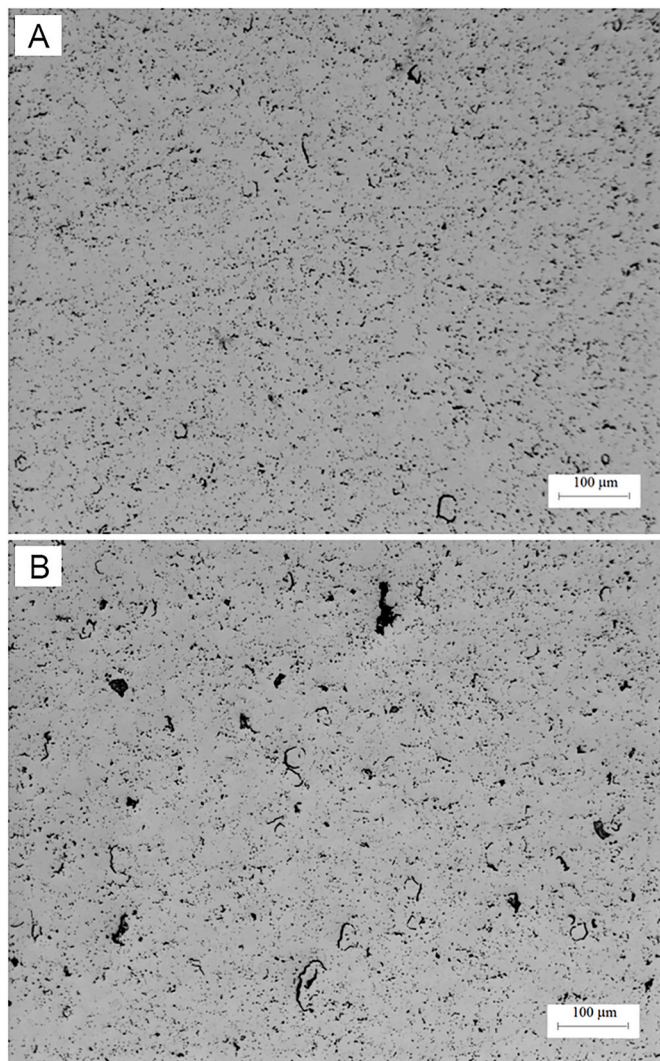


Fig. 9. Light optical microscopy images of (A) pure UO_2 and (B) UO_2 -0.2 wt% ADS sintered pellets. The ADS decomposition caused the formation of large and irregular pores, which decreased the sintered density of UO_2 -0.2 wt%ADS.

These circular involving pores may result from small UO_2 particles agglomerates that shrunk almost entirely separatedly from the matrix. The microstructure from the UO_2 -0.2 wt% ADS sample showed an increased number of these pores, indicating that it is more difficult to break these agglomerates when lubricant is added. Improvements in the homogenization process would allow the formation of a higher density pellet (Klemm and Sobek, 1989) since a more intensive mixture of powders would allow better dispersion of the lubricant around the UO_2 particles, including the small ones.

We can also notice that larger pores with different shapes were formed by adding ADS (Fig. 9B). These pores possibly originated from large and more cohesive ADS agglomerates (see Fig. 5). These agglomerates might not have been broken during the mechanical mixing step (homogenization). After the ADS decomposition (see Fig. 3B), which ends at 650 °C, i.e., before the beginning of sintering shrinkage (see Fig. 7), the volumes initially occupied by the agglomerates became empty, resulting in large voids that are difficult to be eliminated during the subsequent sintering stages. Therefore, the sintered density of UO_2 -0.2 wt%ADS decreased because of the additional porosity formed by the lubricant, which was not well dispersed.

The pore size distributions are presented in Fig. 10. The addition of the solid lubricant slightly increased the pore frequency in two ranges compared with pure UO_2 : 1.0–2.5 μm and 15–34 μm . Conversely, in the

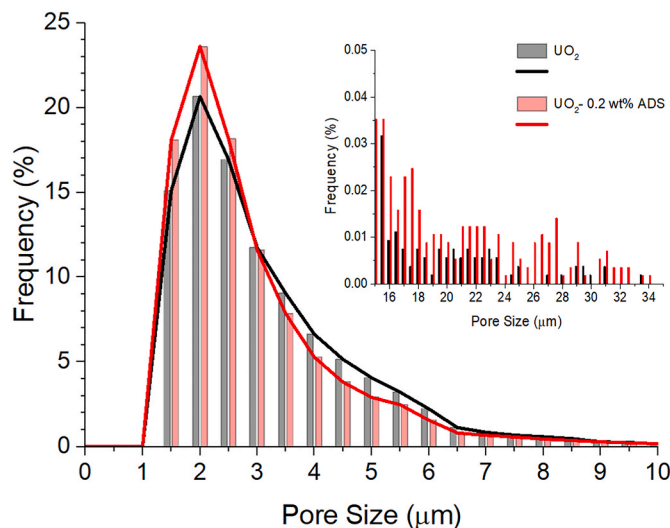


Fig. 10. Pore size distributions of pure UO_2 and UO_2 -0.2 wt%ADS. Insert shows the porosity at 15–31 μm . The solid lubricant increased the pore frequency at 1–2.5 μm and 15–31 μm .

range of 2.5–6.5 μm , higher pore frequencies are present in pure UO_2 . These different distributions resulted in a slightly larger average pore size for the UO_2 pellet.

3.3.2. Grain size analyses

The influence of ADS on grain size distribution is presented in Fig. 11 to Fig. 13 and is summarized in Table 5. Fig. 11A e 11 B show representative microstructures from pure UO_2 and UO_2 -0.2 wt%ADS pellets, respectively. The lubricant addition increased the average grain size from 9.5 μm to 12.8 μm (Table 6). This 35% increase in grain size is low compared to previously reported results (Table 2). We attributed it to the poor mixing of the lubricant, impairing a better dispersion of ADS particles in the UO_2 matrix .

Relative frequency histograms of grain size measurements are presented in Fig. 12. Both distributions started with grains in the same range (2–4 μm), but the ADS addition reduced the frequency of the smaller grains (2–12 μm) and increased the frequency of the larger ones (12–34 μm). In pure UO_2 , the mode (most frequent) and maximum size were 6–8 μm and 32–34 μm , respectively. With ADS addition, both changed to 10–12 μm and 48–50 μm , respectively. The effect of the lubricant is clear at this point: a spread of grain size distribution towards high values. Cumulative frequency curves (Fig. 13) can show this better by comparing D50 values from pure UO_2 (6.8 μm) and UO_2 -0.2 wt%ADS (9.9 μm), i.e., about a 46% increase.

3.4. Thermal stability tests

Thermal stability tests (or resintering) were conducted to assess the out-pile dimensional changes. The densities before and after resintering and the density variations are presented in Table 7. Both variations agree with the industrial specification limits (Costa and Freitas, 2017). The ADS addition enhanced the thermal stability of the fuel since it resintered less (0.46%TD) than the UO_2 (0.55%TD). This behavior might be related to the lower grain boundary area of UO_2 -0.2 wt%ADS (larger grains), impairing the resintering process by reducing the grain boundary diffusion mechanism.

4. Discussion

The observed increase in the shrinkage rate and grain growth might result from the Al^{3+} ions from ADS. However, the mechanism of how aluminum can increase the sintering rate and grain growth is not yet

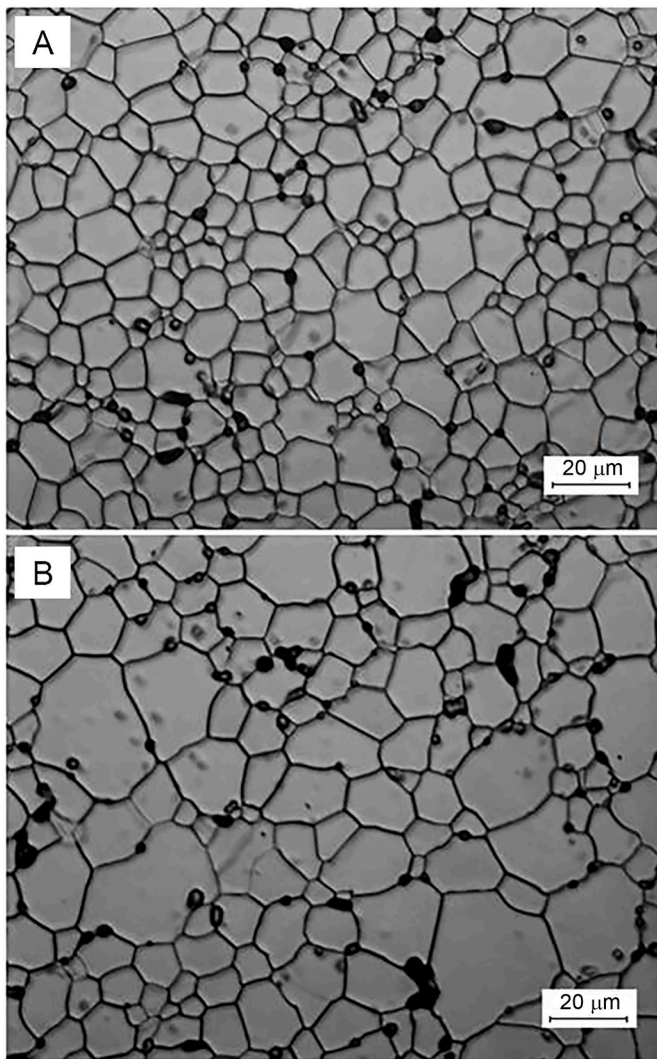


Fig. 11. Light optical microscopy images of (A) pure UO_2 and (B) UO_2 -0.2 wt% ADS sintered pellets. The average grain size increased from 9.5 μm (pure UO_2) to 12.8 μm .

Table 6
Grain size distribution parameters of pure UO_2 and UO_2 -0.2 wt% ADS pellets.

Pellets	Average (μm)	Moda range (μm)	D50 (μm)	Minimum size range (μm)	Maximum size range (μm)
Pure UO_2	9.5	6–8	6.8	2–4	32–34
UO_2 -0.2 wt% ADS	12.8	10–12	9.9	2–4	48–50

Table 7
Values of the sintered and resintered densities and the density variations for pure UO_2 and UO_2 -0.2 wt% ADS.

Samples	Sintered Density (g/cm^3)	Resintered Density (g/cm^3)	Density Variation (%TD)
Pure UO_2	10.61 \pm 0.01	10.67 \pm 0.01	0.55
UO_2 -0.2 wt% ADS	10.55 \pm 0.01	10.60 \pm 0.01	0.46

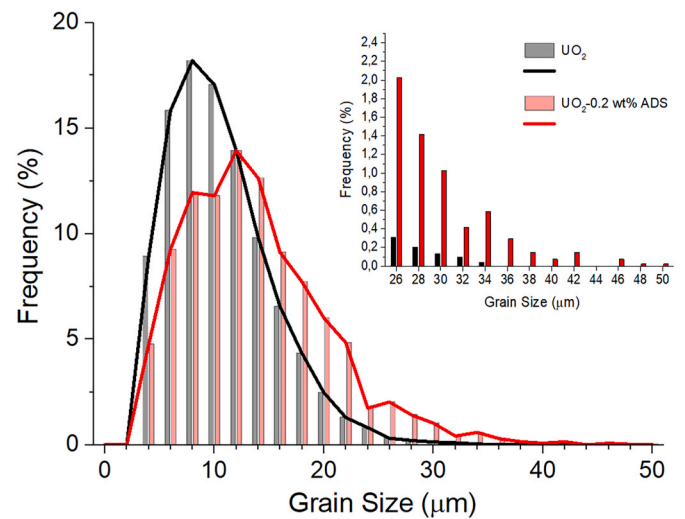


Fig. 12. Grain size distributions of pure UO_2 and UO_2 -0.2 wt% ADS pellets. The addition of ADS reduced the frequency of the smaller grains (2–12 μm) and increased the frequency of the larger ones (12–34 μm).

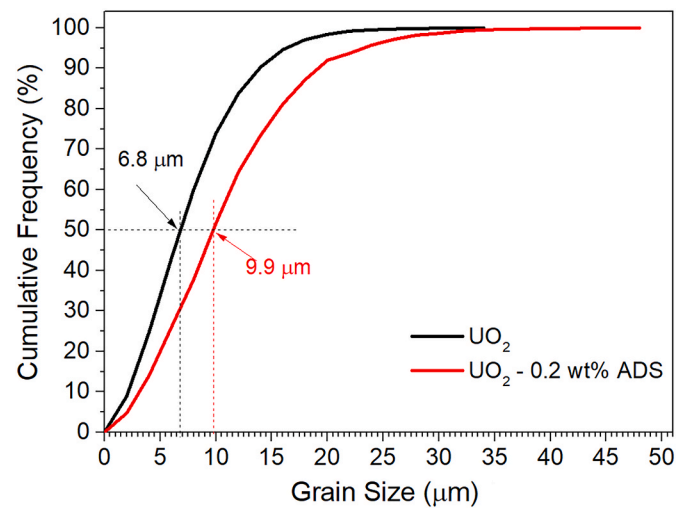


Fig. 13. Cumulative frequencies of grain sizes of pure UO_2 and UO_2 -0.2 wt% ADS pellets. The addition of ADS shifted the D50 toward higher values.

understood. As an attempt to elucidate this mechanism, some analogies with other trivalent cations, e.g., Cr^{3+} and Gd^{3+} , added to UO_2 , can be made, bringing some insights to this subject. When incorporating or doping with aliovalent cations (i.e., cations that differ in charge from the corresponding solvent ion) in UO_2 , some aspects must be considered regarding the resulting changes in the point defects concentration and the solubility of the cation in the host lattice.

Fluorite crystal structure $UO_{2\pm x}$ can be described by three interpenetrating FCC lattices (Keim and Keller, 1986) (or three-ion motif (Bardella et al., 2017)), one for the uranium cations and two for the oxygen anions. The prevalent defects are Frenkel pairs on the anion sublattice (Matzke, 1966). Oxygen vacancies predominate in substoichiometric UO_{2-x} rather than uranium interstitials, while oxygen interstitials predominate in UO_{2+x} rather than uranium vacancies (Matzke, 1981). These variations of stoichiometry are made possible thanks to the ease with which uranium cations may assume different valence states in addition to the U^{4+} state, e.g., U^{3+} , U^{5+} and U^{6+} (Olander, 1976; Keim and Keller, 1986; Liu et al., 2012), with similar energy, as a result of the number of *f* and *d* electrons in its ground states (Ho and Radford, 1986). Charged hyperstoichiometric defects

(quadruple and double negatively charged uranium vacancies and oxygen interstitial, respectively) are readily compensated by the oxidation of U^{4+} to U^{5+} or U^{6+} . The reduction of U^{4+} to U^{3+} demands, however, more energy since high temperatures are needed to reduce UO_2 to UO_{2-x} (Cooper et al., 2018b).

Sintering, or more properly, densification and grain growth depend mainly on the diffusivity of atomic species. Oxygen and uranium diffusion kinetics on UO_2 have been studied for long (Matzke, 1966; Breitung, 1978; Matzke, 1981; Matzke, 1986; Matzke, 1987; Marin and Contamin, 1969; Ando and Oishi, 1983; Atkinson, 1989; Sabioni et al., 2000; Ruello et al., 2004; Berthier et al., 2013; Laik and Kumar Dey, 2017). It was already stated that oxygen diffusivity is much higher than that of uranium (Matzke, 1981, 1986, 1987; Ando and Oishi, 1983; Atkinson, 1989), and self-diffusion coefficients of both the anion and cation are sensitive to the stoichiometry variation (Ando and Oishi, 1983). Since uranium diffusion is slower, this is the rate-limiting step for the whole atomic transport (Matzke, 1986, 1987) and is then a major requirement regarding sintering and grain growth. Uranium diffusivity (in its proper lattice) can be enhanced in two ways. First and more effectively, by creating uranium vacancies since diffusion through them demands less energy. Second, by oxidation of uranium cations U^{4+} to smaller U^{5+} or U^{6+} , having higher diffusivities (Ho and Radford, 1986). However, these point defects are dependent on each other due to the charge balance. Besides, they can be affected by the oxygen potential of the sintering atmosphere. U^{4+} interstitials are expected to self-diffuse in substoichiometric UO_{2-x} (Lidiard, 1966; Matzke, 1986), but a correlation with enhanced sintering is not clear.

A negative effective charge defect is produced when a trivalent substitutional cation is incorporated in UO_2 . Charge compensation can be done by forming oxygen vacancies (in fact, one oxygen vacancy for two substitutional cations) which promotes a decrease in the uranium vacancies by Schottky equilibrium. This is the opposite situation of incorporating a pentavalent substitutional cation (Matzke, 1966).

Chromia (Cr_2O_3) is by far the most studied dopant regarding UO_2 grain growth and enhanced sintering (Killeen, 1980; Peres et al., 1993; Kashibe and Une, 1998; Leenaers et al., 2003; Kim et al., 2003; Arborlious et al., 2006; Middleburgh et al., 2012a, 2012b; Cardinaels et al., 2012; Mieszczyński et al., 2014; Massih and Jernkvist, 2015; Guo et al., 2017). This profusion of experimental and theoretical investigations brings out divergences related to the solid solution type (substitutional or interstitial) and so the resultant charge compensation mechanism for the Cr ions insertion in the UO_2 lattice. Cr substitution for U ions should increase the concentration of oxygen vacancies in hypostoichiometric UO_{2-x} and stoichiometric UO_2 (Middleburgh et al., 2012a, 2012b; Mieszczyński et al., 2014; Massih and Jernkvist, 2015; Guo et al., 2017). Following this, there is a decrease in the concentration of uranium vacancies (through Schottky equilibrium) which is succeeded by an increase in the concentration of uranium interstitials through Frenkel equilibrium. In hyperstoichiometric UO_{2+x} , thanks to the excess of oxygen, charge compensation is accomplished by U^{5+} ions (Middleburgh et al., 2012b), which can also be the case for stoichiometric UO_2 (Cardinaels et al., 2012). As for Cr interstitials, they are justified by Hume-Rotery rules, based on its cationic radius and the size of the interstitial space in UO_2 (Leenaers et al., 2003). By dissolving chromium interstitially, assuming to remain trivalent, the concentration of oxygen interstitials is increased (for charge compensation), and thus the concentration of oxygen vacancies is decreased (through Frenkel equilibrium). Consequently, there is an increase in the concentration of uranium vacancies (through Schottky equilibrium) (Kashibe and Une, 1998; Kim et al., 2003), leading to the oxidation of U^{4+} atoms to U^{5+} to compensate for the charge (Leenaers et al., 2003; Mieszczyński et al., 2014; Guo et al., 2017). The work of Kim et al. (2003) cited here did not specify that chromium is interstitial, but the comments presented agree with that statement (interstitial solution). More recently, a combined density functional theory (DFT) and empirical potential description of defect-free energy (U) were used to calculate the doped UO_2 defect

concentration as a function of temperature. According to this, there is a substitutional to interstitial ratio of Cr atoms that changes as temperature increases during sintering. At high sintering temperatures, Cr can change its valence state from 3+ to 1+, becoming a positively charged interstitial defect, causing an increase in the uranium vacancy concentration and enhancing grain growth (Cooper et al., 2018a). Kim et al. (2003) argued that two mechanisms could explain it depending on the atmosphere (H_2O -to- H_2 ratio). Since Cr_2O_3 can be reduced at about 1670 °C, liquid phase sintering can occur by eutectic formation ($Cr + Cr_2O_3$). It is the case in an atmosphere with an intermediate H_2O/H_2 ratio (1×10^{-2}). However, in an atmosphere with a higher H_2O/H_2 ratio (3×10^{-2}), Cr_2O_3 reduction is not expected, so the observed grain growth was also explained by point defect concentration change. In that case, increased uranium diffusion is accomplished by oxygen interstitials generation, which, in turn, decreases the oxygen vacancy concentration (through Frenkel equilibrium), increasing the uranium vacancy concentration (through Schottky equilibrium). However, no reference was made regarding whether Cr ions were dissolved interstitially or substitutionally in UO_2 .

Gadolinia (Gd_2O_3) is added to UO_2 fuel as a burnable poison or absorber in LWRs, and with regard to this application, it has been extensively studied for more than five decades (Beals and Handwerk, 1965; Littlechild et al., 1973; Ohmichi et al., 1981; Fukushima et al., 1982; Une and Oguma, 1985; Ho and Radford, 1986; Miyake et al., 1986; Assmann et al., 1988; Riella et al., 1991; Kubo et al., 1993; Gündüz and Uslu, 1996; Durazzo and Riella, 2001; Krishnan et al., 2009; Durazzo et al., 2010; Durazzo et al., 2013; Pieck et al., 2015; Kim et al., 2017). Burnable poisons are utilized for in-core fuel management enhancement allowing compensation of the excess reactivity of the fuel at the beginning of its life. However, their presence affects the sintering and grain size of the fuel pellets compared to the pure UO_2 . Contrarily to Cr ions (when doping with Cr_2O_3), there is no controversy about the substitutional dissolution of Gd^{3+} ions in the UO_2 lattice since its size is over 5% larger than the U^{4+} ion radius (Ohmichi et al., 1981; Ho and Radford, 1986). In addition, contrarily to Cr^{3+} ions, Gd^{3+} ions are very stable (Miyake et al., 1986). UO_2 - Gd_2O_3 pellets' sinterability or sintering was seen to be modified by the way gadolinium is incorporated into the fuel, e.g., mechanical blending (Littlechild et al., 1973; Davis and Potter, 1978; Manzel and Dörr, 1980; Ohmichi et al., 1981; Une and Oguma, 1985; Miyake et al., 1986; Ho and Radford, 1986; Arai et al., 1987; Assmann et al., 1988; Kogai et al., 1989; Hirai, 1990; Riella et al., 1991; Kubo et al., 1993; Song et al., 2001; Durazzo and Riella, 2001; Durazzo et al., 2010; Lee et al., 2017) and/or mechanical milling/grinding of both oxide powders (Beals and Handwerk, 1965; Une, 1988; Yuda and Une, 1991; Pieck et al., 2015; Kim et al., 2017), co-precipitation (Wada et al., 1973; Ohmichi et al., 1981; Miyake et al., 1986; Kogai et al., 1989; Hirai, 1990; Riella et al., 1991; Durazzo and Riella, 2001; Durazzo et al., 2010), sol-gel process (Gündüz and Uslu, 1996) or even combustion synthesis (Krishnan et al., 2009). The reason for that is associated with the homogeneity or dispersion degree of gadolinium distribution in the pellet before sintering, as reported before (Durazzo and Riella, 2001).

The degree of homogeneity of gadolinia distributions was concerned very earlier in order to achieve complete solubility in the UO_2 matrix (Littlechild et al., 1973). That is the main reason for introducing milling after UO_2 - Gd_2O_3 powder blending. However, when the gadolinium distribution occurs at an atomic level, e.g., in the case of the coprecipitation route, it was undoubtedly seen that sinterability is increased with Gd content (Riella et al., 1991; Durazzo and Riella, 2001). As homogeneity is decreased, as in the case of mechanical blending of UO_2 and Gd_2O_3 , porosity is generated by the known Kirkendall effect (Smigelskas and Kirkendall, 1947; Seitz, 1953) as reported before (Song et al., 2001; Durazzo et al., 2013). Faster diffusion of gadolinium into the UO_2 phase than uranium in the Gd_2O_3 phase, favored by the higher solubility of Gd_2O_3 in UO_2 , can explain the voids generated at the site of Gd_2O_3 particles, which are formed when sintering is in an advanced stage (closed pores structure), thus impairing densification (Durazzo

et al., 2013). The effect of Gd content on point defect chemistry should then be restricted to the unbiased case provided by the homogeneous Gd distribution at an atomic level. Classical explanation rested on the formation of oxygen vacancies and/or U^{4+} ion oxidation to U^{5+} generated by Gd^{3+} solid solution on UO_2 . As argued in last century's works, particularly from the eighties and nineties (Ohmichi et al., 1981; Ho and Radford, 1986; Hirai, 1990; Riella et al., 1991; Massih et al., 1992; Gündüz and Uslu, 1996), the addition of Gd^{3+} to UO_2 can be compensated by oxygen vacancies and/or oxidation of U^{4+} to U^{5+} , depending on the sintering atmosphere. The higher the oxygen potential of the sintering atmosphere, the higher the U^{5+} ions content will be. The smaller U^{5+} ion compared to U^{4+} has higher mobility which would explain the enhanced densification, even under reduced industrial sintering atmospheres, where the oxygen partial pressure is high enough to keep the hyperstoichiometry of UO_2 (Palanki, 2016). Compensation by oxygen vacancies would decrease the concentration of uranium vacancies considering Schottky equilibrium. So U^{5+} formation must be prevalent and was considered by the reports where increased densification was verified (Ho and Radford, 1986; Riella et al., 1991; Durazzo and Riella, 2001).

As for the effect of Gd content on grain size, there are some divergent data in the literature, no matter what the way gadolinium is added to the fuel (Littlechild et al., 1973; Wada et al., 1973; Ho and Radford, 1986; Kogai et al., 1989; Yuda and Une, 1991; Riella et al., 1991; Gündüz and Uslu, 1996; Massih, 2014; Baena et al., 2015; Liu et al., 2017; Kim et al., 2017; Hirai et al., 1995). Some reports (Ho and Radford, 1986; Yuda and Une, 1991) related a grain size increase with oxygen potential, which is favored by U^{5+} formation. Others yet revealed a variable behavior dependent on the gadolinium content, i.e., a grain size decrease up to certain content followed by an increase above it (Hirai et al., 1995; Littlechild et al., 1973). However, more recent results from Kim et al. (2017) have clearly shown that Gd's major effect on grain growth is deleterious (grain size decreases as Gd content increases). This subject shed light on the fact that what makes the sinterability be enhanced, U^{5+} generation, particularly on hypostoichiometric specimen, lowers the decrease in grain size, but it is not enough to enlarge grain size related to UO_2 as Gd content is increased. The alleged reason presented by Kim et al. (2017) concerning the suppression of U atom diffusion by the fluorite lattice contraction is contradicted by enhanced sinterability results (Ho and Radford, 1986; Riella et al., 1991; Durazzo and Riella, 2001). As observed by Kubo et al. (1993), Gd can be segregated to the grain boundary, impairing the conductivity along this path. If Gd lowers the grain boundary energy, as suggested by Littlechild et al. (1973), this segregation could justify the impairing of grain growth. In fact, sintering theory states that in polycrystalline materials, grain boundary diffusion and lattice diffusion from the grains boundary to the pore are the most important densifying mechanism (Rahaman, 2007). What drives de densification process is the free energy reduction. This reduction is accomplished by both surface and grain boundary area reduction. By grain growth, there is a reduction in the total grain boundary area, which provides an alternative process by which the powder system can decrease its free energy. This alternative process seems to be not operative by adding Gd_2O_3 to UO_2 . The free energy reduction associated with grain growth depends directly on the grain boundary energy (Rahaman, 2007). The higher the grain boundary energy, the higher the free energy reduction associated with it. If gadolinium reduces the grain boundary energy, grain growth in UO_2 - Gd_2O_3 solid solution will be impaired.

As for aluminum, this is a trivalent cation, but different from chromium, its valence does not change when added to UO_2 (Cooper et al., 2018a), so there are no controversial findings about its location on the host lattice: Al^{3+} is a substitutional solute as Cr^{3+} and Gd^{3+} , in spite of having a smaller effective ionic radius (53.5 p.m.) than the others (61.5 and 93.8 p.m., respectively, assuming 6 as the coordination number) (Dean and Lange, 1999). As a substitutional trivalent solute in UO_2 , a similar behavior to Gd^{3+} ions is expected, i.e., a compensation mechanism based on oxygen vacancies generation and/or oxidation of U^{4+} to

U^{5+} . The increased mobility of the U^{5+} ions fits well with the results presented here since it can justify the increased shrinkage rate observed when ADS was added to UO_2 (see Fig. 8). It can also explain the small increase in density reported in previous publications, as summarized in Table 2. There are two reasons for this small increase. First, the solid solubility limit of Al_2O_3 in UO_2 is very small (about 70 ppm) (Bourgeois, 1993), and over that limit, fine precipitation is observed with no effect on U^{5+} generation, which impairs grain growth (Leckie and Luther, 2013). Second, the uranium diffusion rate would increase if uranium vacancies could be generated, as is the case of Nb_2O_5 addition (Radford and Pope, 1983; Une et al., 1987) or Cr_2O_3 addition, considering interstitial chromium ions (Kashibe and Une, 1998; Kim et al., 2003; Cooper et al., 2018a). In our case, final sintered densities were even decreased due to strong agglomerates of ADS, as explained in the results section.

The same charge compensation mechanism, i.e., oxidation of U^{4+} to U^{5+} , has been suggested to explain the grain size effect of aluminum addition in UO_2 . The grain size growth resultant from Al_2O_3 addition is not as high as the Cr_2O_3 addition since the solid solubility limit is one order of magnitude lower than Cr_2O_3 (Bourgeois, 1993). Additions over this limit originate precipitates that hinder grain growth (Leckie and Luther, 2013). Nevertheless, the effect of aluminum addition on grain growth is higher than on densification, as shown in Table 2. So, it seems that there is another cause than oxidation of uranium cations for this behavior. If we look at the effect of Gd_2O_3 addition, there is a reduction in grain size, as discussed above (Kim et al., 2017). In spite of that, when 0.2 wt% of $Al(OH)_3$ was added to UO_2 -7wt% Gd_2O_3 fuel, as reported by Santos et al. (2017), a grain size increase was observed from 4.4 to 10.4 μm (see Table 2). The final grain size is not high but considering that gadolinium decreases the grain size, this result indicates that aluminum may have an opposite role. Since it was argued earlier that gadolinium could reduce the grain boundary energy (Littlechild et al., 1973) and so impair grain growth of the UO_2 - Gd_2O_3 solid solution, we suggest that grain boundary energy is increased by aluminum. Moreover, the aluminum effect on that energy is much stronger than gadolinium in the opposite direction since the quantity added is significantly smaller than that of the nuclear poison. A good dispersion of the dopant is, of course, essential to reach about a 100% increase in grain size, as previously reported (Kashibe and Une, 1998; Lee et al., 2011; Leckie and Luther, 2012, 2013). Otherwise, grain growth will not be so high, resulting in lower values as in the present case (35%).

5. Conclusion

The influence of 0.2 wt%ADS addition on the sintering behavior and microstructure of UO_2 fuel was investigated. The lubricant decreases the total shrinkage from 19.9% (pure UO_2) to 19.4%. Moreover, it causes an increase in the slope of the sintering curve, indicating that the densification is accelerated by its addition. However, large ADS agglomerates form large pores and decrease the final sintered density since these pores cannot be eliminated during sintering. An increment of only ~35% in the average grain size is achieved by the addition of the lubricant. We attributed that to the presence of strong ADS agglomerates, which impaired a good dispersion of the additive.

We also demonstrated that the ADS has an important role during compaction, avoiding ejection defects such as fractures, cracks, and end-capping, representing a significant economic gain for the industry. Furthermore, the results from this study may be a starting point for future developments in using a solid lubricant on an industrial scale.

Based on a literature review of the effects caused by dopants in UO_2 fuel, along with our results, we suggested that aluminum in a solid solution can promote grain growth by increasing the grain boundary energy.

Declaration of competing interest

The authors declare that they have no known competing financial interests or personal relationships that could have appeared to influence the work reported in this paper.

Data availability

Data will be made available on request.

Acknowledgements

Financial support from CAPES was acknowledged. The authors also thank the Nuclear Industries of Brazil (INB, Indústrias Nucleares do Brasil S.A.) for using its facilities and laboratories during this study. DRC is funded by the Swedish Foundation for Strategic Research (SSF, Stiftelsen för Strategisk Forskning). [Project reference number ID17-0078].

References

- Ando, K., Oishi, Y., 1983. Diffusion characteristics of actinide oxides. *J. Nucl. Sci. Technol.* 20 (12), 973–982. <https://doi.org/10.1080/18811248.1983.9733499>.
- Arai, Y., Ohmichi, T., Fukushima, S., Handa, M., 1987. Electrical conductivity of near-stoichiometric (U, Gd)₂O₃ solid solutions. *J. Nucl. Mater.* 150 (2), 233–237. [https://doi.org/10.1016/0022-3115\(87\)90078-X](https://doi.org/10.1016/0022-3115(87)90078-X).
- Arborelius, J., Backman, K., Hallstadius, L., Limbäck, M., Nilsson, J., Rebsdorff, B., Zhou, G., Kitano, K., Löfström, R., Rönnerberg, G., 2006. Advanced doped UO₂ pellets in LWR applications. *J. Nucl. Sci. Technol.* 43 (9), 967–976. <https://doi.org/10.1080/18811248.2006.9711184>.
- Assmann, H., Peehs, M., Roepenack, H., 1988. Survey of binary oxide fuel manufacturing and quality control. *J. Nucl. Mater.* 153 (C), 115–126. [https://doi.org/10.1016/0022-3115\(88\)90202-4](https://doi.org/10.1016/0022-3115(88)90202-4).
- ASTM, 2008. B962-08 - Standard Test Methods for Density of Compacted or Sintered Powder Metallurgy (PM) Products Using Archimedes' Principle. ASTM Int.
- Atkinson, A., 1989. Defects and diffusion in metal oxides. In: *Studies in Inorganic Chemistry*, vol. 9. <https://doi.org/10.1016/B978-0-444-88534-0.50009-6>.
- Baena, A., Cardinaels, T., Vos, B., Binnemans, K., Verwerf, M., 2015. Synthesis of UO₂ and ThO₂ doped with Gd₂O₃. *J. Nucl. Mater.* 461, 271–281. <https://doi.org/10.1016/j.jnucmat.2015.03.028>.
- Balakrishna, P., Asnani, C.K., Kartha, R.M., Ramachandran, K., Sarat Babu, K., Ravichandran, V., Narasimha, M., Ganguly, C., 1999. Uranium dioxide powder preparation, pressing, and sintering for optimum yield. *Nucl. Technol.* 127 (3), 375–381. <https://doi.org/10.13182/NT99-A3007>.
- Bardella, F., Montes Rodrigues, A., Leal Neto, R.M., 2017. CrystalWalk: crystal structures, step by step. *J. Appl. Crystallogr.* 50 (3), 949–950. <https://doi.org/10.1107/S160057671700560X>.
- Beals, R.J., Handwerk, J.H., 1965. Solid solutions in the system urania—rare-earth oxides: I, UO₂-GdO_{1.5}. *J. Am. Ceram. Soc.* 48 (5), 271–274. <https://doi.org/10.1111/j.1151-2916.1965.tb14735.x>.
- Belle, J., 1961. Washington. In: Belle, J., xiii, Pp (Eds.), *Uranium Dioxide: Properties and Nuclear Applications*, p. 726.
- Berthier, C., Rado, C., Chatillon, C., Hodaj, F., 2013. Thermodynamic assessment of oxygen diffusion in non-stoichiometric UO_{2±x} from experimental data and Frenkel pair modeling. *J. Nucl. Mater.* 433 (1–3), 265–286. <https://doi.org/10.1016/j.jnucmat.2012.09.011>.
- Bourgeois, L., 1993. Contribution à l'étude du rôle de dopants dans la densification et la croissance cristalline du dioxyde d'uranium. Report CEA-R-5621. 145pp.
- Breitung, W., 1978. Oxygen self and chemical diffusion coefficients in. *J. Nucl. Mater.* 74 (1), 10–18. [https://doi.org/10.1016/0022-3115\(78\)90527-5](https://doi.org/10.1016/0022-3115(78)90527-5).
- Cardinaels, T., Govers, K., Vos, B., Van Den Berghe, S., Verwerf, M., De Tollenaere, L., Maier, G., Delafoy, C., 2012. Chromia doped UO₂ fuel: investigation of the lattice parameter. *J. Nucl. Mater.* 424 (1–3), 252–260. <https://doi.org/10.1016/j.jnucmat.2012.02.025>.
- Cooper, M.W.D., Stanek, C.R., Andersson, D.A., 2018a. The role of dopant charge state on defect chemistry and grain growth of doped UO₂. *Acta Mater.* 150, 403–413. <https://doi.org/10.1016/j.actamat.2018.02.020>.
- Cooper, M.W.D., Murphy, S.T., Andersson, D.A., 2018b. The defect chemistry of UO_{2±x} from atomistic simulations. *J. Nucl. Mater.* 504, 251–260. <https://doi.org/10.1016/j.jnucmat.2018.02.034>.
- Costa, D.R., Ezequiel, F.J., Gonzaga, R., Bernardelli, S.H., 2013. Individual influence of Al₂O₃ and Nb₂O₅ on grain growth of UO₂ sintered pellets manufactured at INB [Online]. Available: <http://www.iaea.org/inis/collection/NCLCollectionStore/Public/45/087/45087491.pdf?r=1>.
- Costa, D.R., Freitas, A.C., 2017. Thermal stability test of UO₂-doped pellet manufactured at INB. In: *International Nuclear Atlantic Conference - INAC* [Online]. Available: <https://inis.iaea.org/collection/NCLCollectionStore/Public/49/018/49018178.pdf>.
- Davis, H.H., Potter, R.A., 1978. UO₂-Gd₂O₃ Sintering behavior. In: *Processing of Crystalline Ceramics*, pp. 515–524. https://doi.org/10.1007/978-1-4684-3378-4_43.
- Dean, J.A., Lange, N.A., 1999. Lange's Handbook of Chemistry, fifteenth ed. Retrieved from: <https://books.google.com.br/books?id=56KPMQEACAAJ>.
- Delafoy, C., Dewes, P., 2006. AREVA NP New UO₂ fuel development and qualification for LWRs applications. *Proceedings of TopFuel (1)*, 487–491. Retrieved from: https://inis.iaea.org/search/search.aspx?orig_q=RN:44095115.
- Durazzo, M., Riella, H.G., 2001. Effect of mixed powder homogeneity on the UO₂-Gd₂O₃ nuclear fuel sintering behavior. *Key Eng. Mater.* 189–191, 60–66. <https://doi.org/10.4028/www.scientific.net/KEM.189-191.60>.
- Durazzo, M., Oliveira, F.B.V., Urano De Carvalho, E.F., Riella, H.G., 2010. Phase studies in the UO₂-Gd₂O₃ system. *J. Nucl. Mater.* 400 (3), 183–188. <https://doi.org/10.1016/j.jnucmat.2010.03.001>.
- Durazzo, M., Saliba-Silva, A.M., Urano De Carvalho, E.F., Riella, H.G., 2013. Sintering behavior of UO₂-Gd₂O₃ fuel: pore formation mechanism. *J. Nucl. Mater.* 433 (1–3), 334–340. <https://doi.org/10.1016/j.jnucmat.2012.09.033>.
- Durazzo, M., Freitas, A.C., Sansone, A.E.S., Ferreira, N.A.M., de Carvalho, E.F.U., Riella, H.G., Leal Neto, R.M., 2018. Sintering behavior of UO₂Er₂O₃ mixed fuel. *J. Nucl. Mater.* 510, 603–612. <https://doi.org/10.1016/j.jnucmat.2018.08.051>.
- Filipot, A.J., Delbrassine, A., Gilissen, R., 1973. Behaviour of uranium oxide fuel containing burnable poisons. Symposium on the Results of Five Years of BR2 Reactor Utilization. Retrieved from: <https://www.osti.gov/servlets/purl/4264523>.
- Fukushima, S., Ohmichi, T., Maeda, A., Watanabe, H., 1982. The effect of gadolinium content on the thermal conductivity of near-stoichiometric (U,Gd)₂O₃ solid solutions. *J. Nucl. Mater.* 105 (2–3), 201–210. [https://doi.org/10.1016/0022-3115\(82\)90375-0](https://doi.org/10.1016/0022-3115(82)90375-0).
- Gündüz, G., Uslu, I., 1996. Powder characteristics and microstructure of uranium dioxide and uranium dioxide-gadolinium oxide fuel. *J. Nucl. Mater.* 231 (1–2), 113–120. [https://doi.org/10.1016/0022-3115\(96\)00349-2](https://doi.org/10.1016/0022-3115(96)00349-2).
- Guo, Z., Ngayam-Happy, R., Krack, M., Pautz, A., 2017. Atomic-scale effects of chromium-doping on defect behaviour in uranium dioxide fuel. *J. Nucl. Mater.* 488, 160–172. <https://doi.org/10.1016/j.jnucmat.2017.02.043>.
- Hirai, M., 1990. Thermal diffusivity of UO₂-Gd₂O₃ pellets. *J. Nucl. Mater.* 173 (3), 247–254. [https://doi.org/10.1016/0022-3115\(90\)90392-Z](https://doi.org/10.1016/0022-3115(90)90392-Z).
- Hirai, M., Davies, J.H., Williamson, R., 1995. Diffusivities of fission gas species in UO₂ and (U,Gd)₂O₃ nuclear fuels during irradiation. *J. Nucl. Mater.* 226 (1–2), 238–251. [https://doi.org/10.1016/0022-3115\(95\)00091-7](https://doi.org/10.1016/0022-3115(95)00091-7).
- Ho, S.M., Radford, K.C., 1986. Structural chemistry of solid solutions in the UO₂-Gd₂O₃ system. *Nucl. Technol.* 73 (3), 350–360. <https://doi.org/10.13182/NT86-A16077>.
- Hua, D., Yongzhong, Z., Xuemin, Y.A.N., 2004. Yibin nuclear fuel element plant's experience in manufacturing of large grain size pellet. IAEA-TECDOC-1416, 155–160. Retrieved from *Advanced Fuel Pellet Materials and Designs for Water Cooled Reactors*. <https://www.iaea.org/publications/7056/advanced-fuel-pellet-materials-and-designs-for-water-cooled-reactors>.
- IAEA – International Atomic Energy Agency, 2012. IAEA-Tecdoc-1686. Retrieved from *Experiences and trends of manufacturing technology of advanced nuclear fuel*. http://www-pub.iaea.org/MTCD/Publications/PDF/TE_1686_web.pdf.
- Jentzen, W.R., Didway, J.A., 1990. Method of Making a UO₂ Fuel Pellet. Retrieved from: <https://patents.google.com/patent/EP0395979A1>.
- Kang, K.W., Yang, J.H., Kim, J.H., Rhee, Y.W., Kim, D.J., Kim, K.S., Song, K.W., 2010. Effects of MnO-Al₂O₃ on the grain growth and high-temperature deformation strain of UO₂ fuel pellets. *J. Nucl. Sci. Technol.* 47 (3), 304–307. <https://doi.org/10.1080/18811248.2010.9711958>.
- Kashibe, S., Une, K., 1998. Effect of additives (Cr₂O₃, Al₂O₃, SiO₂, MgO) on diffusional release of ¹³³Xe from UO₂ fuels. *J. Nucl. Mater.* 254 (2–3), 234–242. [https://doi.org/10.1016/S0022-3115\(97\)00356-5](https://doi.org/10.1016/S0022-3115(97)00356-5).
- Keim, R., Keller, C. (Eds.), 1986. *Gmelin Handbook of Inorganic Chemistry – Uranium Supplement*, eighth ed., C5. –Springer-Verlag, p. 260. <https://doi.org/10.1007/978-3-662-10716-4>.
- Killeen, J.C., 1980. Fission gas release and swelling in UO₂ doped with Cr₂O₃. *J. Nucl. Mater.* 88 (2–3), 177–184. [https://doi.org/10.1016/0022-3115\(80\)90272-X](https://doi.org/10.1016/0022-3115(80)90272-X).
- Kim, K.S., Song, K.W., Yang, J.H., Kang, K.W., Jung, Y.H., 2003. Sintering behavior of Cr₂O₃-doped UO₂ pellets. *Journal of the Korean Nuclear Society* 35 (1), 14–24. Retrieved from: <https://www.kns.or.kr/files/jour/v35/A04803285988.pdf>.
- Kim, D., 2007. Effect of Sintering Condition on the Grain Growth of an Al-Doped UO₂ Pellet. *Transactions of the Korean Nuclear Society Spring Meeting, Jeju, Korea*, pp. 10–11.
- Kim, J., Lee, J., Youn, Y.S., Liu, N., Kim, J.G., Ha, Y.K., Kim, J.Y., 2017. The Combined influence of gadolinium doping and non-stoichiometry on the structural and electrochemical properties of uranium dioxide. *Electrochim. Acta* 247, 942–948. <https://doi.org/10.1016/j.electacta.2017.07.023>.
- Klemm, U., Sobek, D., 1989. Influence of admixing of lubricants on compressibility and compactibility of uranium dioxide powders. *Powder Technol.* 57 (2), 135–142. [https://doi.org/10.1016/0032-5910\(89\)80017-8](https://doi.org/10.1016/0032-5910(89)80017-8).
- Kogai, T., Iwasaki, R., Hirai, M., 1989. In-pile and out-of-pile grain growth behavior of sintered UO₂ and (U,Gd)₂O₃ pellets. *J. Nucl. Sci. Technol.* 26 (8), 744–751. <https://doi.org/10.1080/18811248.1989.9734378>.
- Krishnan, R.V., Panneerselvam, G., Manikandan, P., Antony, M.P., Nagarajan, K., 2009. Heat capacity and thermal expansion of uranium-gadolinium mixed oxides. *J. Nucl. Radiochem. Sci.* 10 (1), 19–26. <https://doi.org/10.14494/jnrs.10.1.19>.
- Kubo, T., Ishimoto, S., Koyama, T., 1993. Effects of gadolinium doping on electrical properties of UO₂ grain boundaries. *J. Nucl. Sci. Technol.* 30 (7), 664–672. <https://doi.org/10.1080/18811248.1993.9734532>.
- Laik, A., Kumar Dey, G., 2017. Diffusion in nuclear materials. *Handbook of Solid State Diffusion* 2, 339–377. <https://doi.org/10.1016/b978-0-12-804548-0.00008-6>.
- Leckie, R.M., Luther, E.P., 2012. Report on controlling the microstructure of UO₂ pellets. LA-Report UR-12-24919. <https://doi.org/10.2172/1052369>.

- Leckie, R.M., Luther, E.P., 2013. Report on Evolutionary Enhancements to UO₂ Pellets. LA-Report UR-13-22252. <https://doi.org/10.2172/1072232>.
- Lee, S., Jung, D., Lee, C., Kim, J., Jeon, K., Lee, J., Yang, J., Kim, K., 2011. Fabrication and Characteristic Tests of the Large Grain UO₂ Pellets for HIPER Fuel. Water Reactor Fuel Performance Meeting, paper ID T1 016, Chengdu - China.
- Lee, J., Kim, J., Youn, Y.S., Liu, N., Kim, J.G., Ha, Y.K., Kim, J.Y., 2017. Raman study on structure of U_{1-x}Gd_xO_{2-x} (y=0.005, 0.01, 0.03, 0.05 and 0.1) solid solutions. J. Nucl. Mater. 486, 216–221. <https://doi.org/10.1016/j.jnucmat.2017.01.004>.
- Leenaers, A., De Tollenaere, L., Delafay, C., Van den Berghe, S., 2003. On the solubility of chromium sesquioxide in uranium dioxide fuel. J. Nucl. Mater. 317 (1), 62–68. [https://doi.org/10.1016/S0022-3115\(02\)01693-8](https://doi.org/10.1016/S0022-3115(02)01693-8).
- Lidiard, A.B., 1966. Self-diffusion of uranium in UO₂. J. Nucl. Mater. 19 (1), 106–108. [https://doi.org/10.1016/0022-3115\(66\)90138-3](https://doi.org/10.1016/0022-3115(66)90138-3).
- Littlechild, J.E., Butler, G.G., Lester, G.W., 1973. The production of burnable poison oxide fuel. In: Nuclear Fuel Performance. Thomas Telford Publishing, pp. 65.1–65.4. [https://doi.org/10.1016/0022-3115\(73\)90116-2](https://doi.org/10.1016/0022-3115(73)90116-2).
- Liu, X.Y., Andersson, D.A., Uberuaga, B.P., 2012. First-principles DFT modeling of nuclear fuel materials. J. Mater. Sci. 47 (21), 7367–7384. <https://doi.org/10.1007/s10853-012-6471-6>.
- Liu, N., Kim, J., Lee, J., Youn, Y.S., Kim, J.G., Kim, J.Y., Shoesmith, D.W., 2017. Influence of Gd doping on the structure and electrochemical behavior of UO₂. Electrochim. Acta 247, 496–504. <https://doi.org/10.1016/j.electacta.2017.07.006>.
- Lyons, M.F., Boyle, R.F., Davies, J.H., Hazel, V.E., Rowland, T.C., 1972. UO₂ properties affecting performance. Nucl. Eng. Des. 21 (2), 167–199. [https://doi.org/10.1016/0029-5493\(72\)90072-6](https://doi.org/10.1016/0029-5493(72)90072-6).
- Maier, G., Assmann, H., Dörr, W., 1988. Resinter testing in relation to in-pile densification. J. Nucl. Mater. 153 (C), 213–220. [https://doi.org/10.1016/0022-3115\(88\)90213-9](https://doi.org/10.1016/0022-3115(88)90213-9).
- Manzel, R., Dörr, W.O., 1980. Manufacturing and irradiation experience with UO₂/Gd₂O₃ fuel. Am. Ceram. Soc. Bull. 59 (6), 601–603. Retrieved from. <https://www.osti.gov/biblio/5280816>.
- Marin, J.F., Contamin, P., 1969. Uranium and oxygen self-diffusion in UO₂. J. Nucl. Mater. 30 (1–2), 16–25. [https://doi.org/10.1016/0022-3115\(69\)90164-0](https://doi.org/10.1016/0022-3115(69)90164-0).
- Massih, A.R., Persson, S., Weiss, Z., 1992. Modelling of (U,Gd)O₂ fuel behaviour in boiling water reactors. J. Nucl. Mater. 188, 323–330. [https://doi.org/10.1016/0022-3115\(92\)90492-4](https://doi.org/10.1016/0022-3115(92)90492-4).
- Massih, A.R., 2014. Effects of Additives on Uranium Dioxide Fuel Behavior. Report 2014: 21. Retrieved from. <https://www.stralsakerhetsmyndigheten.se/en/publications/reports/safety-at-nuclear-power-plants/2014/201421/>.
- Massih, A.R., Jernkvist, L.O., 2015. Effect of additives on self-diffusion and creep of UO₂. Comput. Mater. Sci. 110, 152–162. <https://doi.org/10.1016/j.commatsci.2015.08.005>.
- Massih, A.R., Jernkvist, L.O., 2021. Effects of Additives on UO₂ Fuel Behavior, expanded edition. Report 2021:20. Retrieved from. <https://www.stralsakerhetsmyndigheten.se/publikationer/rapporter/sakerhet-vid-karnkraftverken/2021/202120/>.
- Matsuda, T., Yuasa, Y., Kobayashi, S., Toba, M., 1998. Characteristics of fuel pellet with additive of Al and Si. IAEA-TECDOC-1036, 9–18. Retrieved from Advances in Fuel Pellet Technology for Improved Performance at High Burnup. <https://www.iaea.org/publications/5333/advances-in-fuel-pellet-technology-for-improved-performance-at-high-burnup>.
- Matzke, H., 1966. Diffusion in doped UO₂. Nucl. Appl. 2 (2), 131–137. <https://doi.org/10.13182/NT66-A27493>.
- Matzke, H., 1981. 4-Diffusion in nonstoichiometric oxides. In: O. Toft Sørensen, Nonstoichiometric Oxides. Academic Press, pp. 155–232. <https://doi.org/10.1016/B978-0-12-655280-5.50009-2>.
- Matzke, H., 1986. Diffusion processes in nuclear fuels. J. Less Common Met. 121, 537–564. [https://doi.org/10.1016/0022-5088\(86\)90573-4](https://doi.org/10.1016/0022-5088(86)90573-4).
- Matzke, H., 1987. Atomic transport properties in UO₂ and mixed oxides (U,Pu)O₂. J. Chem. Soc., Faraday Trans. 2 (7), 1121. <https://doi.org/10.1039/f29878301121>.
- Middleburgh, S.C., Parfitt, D.C., Grimes, R.W., Dorado, B., Bertolus, M., Blair, P.R., Backman, K., 2012a. Solution of trivalent cations into uranium dioxide. J. Nucl. Mater. 420 (1–3), 258–261. <https://doi.org/10.1016/j.jnucmat.2011.10.006>.
- Middleburgh, S.C., Grimes, R.W., Desai, K.H., Blair, P.R., Hallstadius, L., Backman, K., Van Uffelen, P., 2012b. Swelling due to fission products and additives dissolved within the uranium dioxide lattice. J. Nucl. Mater. 427 (1–3), 359–363. <https://doi.org/10.1016/j.jnucmat.2012.03.037>.
- Mieszczynski, C., Kuri, G., Degueldre, C., Martin, M., Bertsch, J., Borca, C.N., Simoni, E., 2014. Irradiation effects and micro-structural changes in large grain uranium dioxide fuel investigated by micro-beam X-ray diffraction. J. Nucl. Mater. 444 (1–3), 274–282. <https://doi.org/10.1016/j.jnucmat.2013.09.054>.
- Miyake, C., Kanamaru, M., Imoto, S., 1986. Microcharacterization of gadolinium in U_{1-x}Gd_xO₂ by means of electron spin resonance. J. Nucl. Mater. 137 (3), 256–260. [https://doi.org/10.1016/0022-3115\(86\)90228-X](https://doi.org/10.1016/0022-3115(86)90228-X).
- OECD Nuclear Energy Agency, 2014. Uranium 2014: resources, production and demand (the red book). In: OECD-NEA. Retrieved from. <https://www.oecd-neo.org/jcms/pl14916>.
- Ohmichi, T., Fukushima, S., Maeda, A., Watanabe, H., 1981. On the relation between lattice parameter and O/M ratio for uranium dioxide-trivalent rare earth oxide solid solution. J. Nucl. Mater. 102 (1–2), 40–46. [https://doi.org/10.1016/0022-3115\(81\)90544-4](https://doi.org/10.1016/0022-3115(81)90544-4).
- Olander, D.R., 1976. Fundamental Aspects of Nuclear Reactor Fuel Elements. <https://doi.org/10.2172/7343826>.
- Olander, D.R., 2009. Nuclear fuels - present and future. J. Nucl. Mater. 389 (1), 1–22. <https://doi.org/10.1016/j.jnucmat.2009.01.297>.
- Palanki, B., 2016. Fabrication of UO₂-Gd₂O₃ fuel pellets. J. Mater. Sci. Chem. Eng. 4 (2), 8–21. <https://doi.org/10.4236/msce.2016.42002>.
- Peres, V., Bourgeois, L., Dehaut, P., 1993. Grain growth and Ostwald ripening in chromia-doped uranium dioxide. J. Phys. IV 3 (C7), 1477–1480. <https://doi.org/10.1051/jp4:19937231>.
- Pieck, D., Desgranges, L., Matheron, P., Palancher, H., 2015. Evidence of a new crystalline phase in U-Gd-O phase diagram. J. Nucl. Mater. 461, 186–192. <https://doi.org/10.1016/j.jnucmat.2015.03.010>.
- Radford, K.C., Pope, J.M., 1983. UO₂ fuel pellet microstructure modification through impurity additions. J. Nucl. Mater. 116 (2–3), 305–313. [https://doi.org/10.1016/0022-3115\(83\)90116-2](https://doi.org/10.1016/0022-3115(83)90116-2).
- Rahaman, M.N., 2007. Sintering of Ceramics (First). Retrieved from. <https://www.routledge.com/Sintering-of-Ceramics/Rahaman/p/book/9780849372865>.
- Rest, J., Cooper, M.W.D., Spino, J., Turnbull, J.A., Van Uffelen, P., Walker, C.T., 2019. Fission gas release from UO₂ nuclear fuel: a review. J. Nucl. Mater. 513, 310–345. <https://doi.org/10.1016/j.jnucmat.2018.08.019>.
- Riella, H.G., Durazzo, M., Hirata, M., Nogueira, R.A., 1991. UO₂-Gd₂O₃ solid solution formation from wet and dry processes. J. Nucl. Mater. 178 (2–3), 204–211. [https://doi.org/10.1016/0022-3115\(91\)90387-M](https://doi.org/10.1016/0022-3115(91)90387-M).
- Ruello, P., Chirlesan, G., Petot-Ervas, G., Petot, C., Desgranges, L., 2004. Chemical diffusion in uranium dioxide - influence of defect interactions. J. Nucl. Mater. 325 (2–3), 202–209. <https://doi.org/10.1016/j.jnucmat.2003.12.007>.
- Sabioni, A.C.S., Ferraz, W.B., Millot, F., 2000. Effect of grain-boundaries on uranium and oxygen diffusion in polycrystalline UO₂. J. Nucl. Mater. 278 (2), 364–369. [https://doi.org/10.1016/S0022-3115\(99\)00250-0](https://doi.org/10.1016/S0022-3115(99)00250-0).
- Santos, L.R., Durazzo, M., Urano de Carvalho, E.F., Riella, H.G., 2017. Effect of Al(OH)₃ on the sintering of UO₂-Gd₂O₃ fuel pellets with addition of U₃O₈ from recycle. J. Nucl. Mater. 493, 30–39. <https://doi.org/10.1016/j.jnucmat.2017.05.050>.
- Schafer, R., Mathieu, V., Gradel, G., Dorr, W., Peehs, M., Assmann, H., 1984. Process for Manufacturing Oxidic Nuclear-Fuel Sintered Bodies. European Patent 0136665B1.
- Seitz, F., 1953. On the porosity observed. Acta Metall. 1 (3), 355–369.
- Shiba, S., 1961. Differential thermal analysis of aluminum soaps. Bull. Chem. Soc. Jpn. 24 (6), 804–809. <https://doi.org/10.1246/bcsj.34.804>.
- Smigelskas, A.D., Kirkendall, E.O., 1947. Zinc diffusion in alpha brass (1942). Trans. AIME 171, 130–142.
- Song, K.W., Sik Kim, K., Ho Yang, J., Won Kang, K., Ho Jung, Y., 2001. A mechanism for the sintered density decrease of UO₂-Gd₂O₃ pellets under an oxidizing atmosphere. J. Nucl. Mater. 288 (2–3), 92–99. [https://doi.org/10.1016/S0022-3115\(00\)00721-2](https://doi.org/10.1016/S0022-3115(00)00721-2).
- Tonks, M., Andersson, D., Devanathan, R., Dubourg, R., El-Azab, A., Freyss, M., Iglesias, F., Kulacsy, K., Pastore, G., Phillip, S.R., Welland, M., 2018. Unit mechanisms of fission gas release: current understanding and future needs. J. Nucl. Mater. 504, 300–317. <https://doi.org/10.1016/j.jnucmat.2018.03.016>.
- Turnbull, J.A., 1974. The effect of grain size on the swelling and gas release properties of UO₂ during irradiation. J. Nucl. Mater. 50 (1), 62–68. [https://doi.org/10.1016/0022-3115\(74\)90061-0](https://doi.org/10.1016/0022-3115(74)90061-0).
- Une, K., Oguma, M., 1985. Oxygen potential of U_{0.96}Gd_{0.04}O₂ (UO₂-3wt% Gd₂O₃) solid solution. J. Nucl. Mater. 131 (1), 88–91. [https://doi.org/10.1016/0022-3115\(85\)90428-3](https://doi.org/10.1016/0022-3115(85)90428-3).
- Une, K., Tanabe, I., Oguma, M., 1987. Effects of additives and the oxygen potential on the fission gas diffusion in UO₂ fuel. J. Nucl. Mater. 150 (1), 93–99. [https://doi.org/10.1016/0022-3115\(87\)90097-3](https://doi.org/10.1016/0022-3115(87)90097-3).
- Une, K., 1988. Effect of oxygen potential on the initial sintering of UO₂ and UO₂-Gd₂O₃ compacts. J. Nucl. Mater. 158 (C), 210–216. [https://doi.org/10.1016/0022-3115\(88\)90170-5](https://doi.org/10.1016/0022-3115(88)90170-5).
- Une, K., Hirai, M., Nogita, K., Hosokawa, T., Suzawa, Y., Shimizu, S., Etoh, Y., 2000. Rim structure formation and high burnup fuel behavior of large-grained UO₂ fuels. J. Nucl. Mater. 278 (1), 54–63. [https://doi.org/10.1016/S0022-3115\(99\)00214-7](https://doi.org/10.1016/S0022-3115(99)00214-7).
- Wada, T., Noro, K., Tsukui, K., 1973. Behaviour of UO₂-Gd₂O₃ fuel. In: Nuclear Fuel Performance, pp. 63.1–63.3. [https://www.scrip.org/\(S\(lz5mqp453edn p55rrgict55.\)\)reference/referencespapers.aspx?referenceid=1668592](https://www.scrip.org/(S(lz5mqp453edn p55rrgict55.))reference/referencespapers.aspx?referenceid=1668592).
- Yang, J.H., Kang, K.W., Kim, K.S., Rhee, Y.W., Song, K.W., 2010. Recycling process for Sinter-Active U₃O₈ powders. J. Nucl. Sci. Technol. 47 (6), 538–541. <https://doi.org/10.1080/18811248.2010.9711976>.
- Yaws, C.L., 2015. Physical properties – organic compounds. In: The Yaws Handbook of Physical Properties for Hydrocarbons and Chemicals. <https://doi.org/10.1016/B978-0-12-800834-8.00001-3>.
- Yuda, R., Une, K., 1991. Effect of sintering atmosphere on the densification of UO₂Gd₂O₃ compacts. J. Nucl. Mater. 178 (2–3), 195–203. [https://doi.org/10.1016/0022-3115\(91\)90386-L](https://doi.org/10.1016/0022-3115(91)90386-L).
- Yuda, R., Harada, H., Hirai, M., Hosokawa, T., Une, K., Kashibe, S., Kubo, T., 1997. Effects of pellet microstructure on irradiation behavior of UO₂ fuel. J. Nucl. Mater. 248, 262–267. [https://doi.org/10.1016/S0022-3115\(97\)00122-0](https://doi.org/10.1016/S0022-3115(97)00122-0).
- Zhong, Y., Gao, R., Li, B., Yang, Z., Huang, Q., Wang, Z., Li, R., 2021. Preparation and characterization of large grain UO₂ for accident tolerant fuel. Frontiers in Materials 8 (April), 1–12. <https://doi.org/10.3389/fmats.2021.651074>.